

Chapter 7

Fabrication of High Performance UVC LEDs on Aluminum-Nitride Semiconductor Substrates and Their Potential Application in Point-of-Use Water Disinfection Systems

James R. Grandusky, Rajul V. Randive, Therese C. Jordan and Leo J. Schowalter

Abstract Water disinfection has always been a focal point of public discourse due to both the shortage of water and the abundance of water-transmitted diseases. According to the World Health Organization (WHO), there are over 3.4 million reported deaths annually due to water, sanitation, and hygiene-related issues [1]. There are a number of technologies being developed to fight against issues related to waterborne diseases. The use of UV light is gaining popularity over chlorine disinfection due to a lack of aftertaste and harmful by-products after treatment. Specifically, UV radiation in the wavelength range of 250–280 nm (UVC) has been shown to effectively disinfect water. Current UVC technology, which uses low and medium pressure mercury lamps, is hampered by the use of fragile quartz housings, long warm up times, and the toxicity of mercury [2]. There is tremendous development happening in the field of semiconductor-based UVC LED technology. This technology can be efficient, cost-effective, and an environmentally friendlier alternative to traditional UVC technology. Emerging $\text{Al}_x\text{Ga}_{1-x}\text{N}$ and AlN -based UVC light-emitting diodes (LEDs) provide many advantages over mercury lamps—including design flexibility, low power consumption, and environmentally friendly construction [3]. Unlike low-pressure mercury lamp technology, which is limited to an emission wavelength near 254 nm, LEDs can be tailored to specific wavelengths throughout the UVC range. UVC LEDs are being developed for disinfection in the 265 nm wavelength range and are showing tremendous progress in power output and device lifetime [4]. This progress has been driven by the relatively recent development of high quality, single-crystal AlN substrates. These AlN substrates allow the growth of pseudomorphic $\text{Al}_x\text{Ga}_{1-x}\text{N}$ device layers with very low defect densities.

J.R. Grandusky · R.V. Randive · T.C. Jordan · L.J. Schowalter (✉)
Crystal IS, 70 Cohoes Avenue, Green Island, NY 12183, USA
e-mail: leo@cisuvc.com

R.V. Randive
e-mail: randive@cisuvc.com

These low defect densities have resulted in improvements in efficiency and power as discussed in this chapter. In addition, UVC LEDs emit radiation in a very different pattern than mercury lamps or other UVC sources that they are replacing. For instance, the LEDs can be designed to emit in a “Lambertian” pattern, allowing the LED to be imaged as a near point source. Using UVC LEDs in water disinfection requires substantial rethinking in the arrangement of UVC radiation sources to achieve an efficient system. In this chapter, we will discuss some of the important parameters necessary for successful flow cell design. The chapter will show the design flexibility offered by UVC LEDs, with some examples of potential designs examined through optical modeling. We will also review some of the recent progress in improving UVC LEDs through pseudomorphic growth of $\text{Al}_x\text{Ga}_{1-x}\text{N}$ on single crystal AlN substrates.

7.1 Introduction

LEDs have entered mainstream lighting due to their significant benefits. Compared to traditional lighting sources, such as incandescent light bulbs and fluorescent light tubes, LEDs are environmentally friendly, wavelength specific and provide high optical output, long lifetime, low power consumption, and low maintenance costs.

Similarly, UVC LEDs are poised to begin replacing mercury lamps and other sources of UVC radiation. The UVC radiation is used either in combination with traditional chemical treatment with chlorine to disinfect drinking water, or instead of chemical treatment, because of the formation of chemical by-products and some chlorine resistant microorganisms.

7.1.1 *Types of UVC Light Sources*

In general, UVC light can be produced by the following variety of lamps:

- Low-pressure (LP) mercury vapor lamps
- Medium pressure (MP) mercury vapor lamps
- Metal Halide lamps
- Xenon Lamps (pulsed UV)
- Deuterium Lamps
- UVC LEDs

UVC LEDs, as semiconductor light sources, are an emerging technology and their use in large-scale manufacturing is new. Their benefits, including environmentally friendly construction, low power consumption, low maintenance costs, and wavelength specificity, are driving an increased focus on this new technology [5].

Advantages of using UVC over chlorine disinfection:

- UVC cannot be overdosed
- No by-products or toxins
- No volatile organic compound (VOC) emissions or toxic air emissions
- Does not require storage of hazardous material
- Requires minimal space for equipment and contact chamber
- Does not affect the smell, taste, or minerals in the water

7.1.2 What Is UVC Light?

Ultraviolet (UV) light, the wavelength range of 100–400 nm, is a component of sunlight that falls in the region between visible light and X-rays of the electromagnetic spectrum (Fig. 7.1). The UV light can further be categorized into separate regions as follows [6]:

- Far UV (or “vacuum”) 100–220 nm
- UVC 220–280 nm
- UVB 280–315 nm
- UVA 315–400 nm

Of these UV regions, UVC has significant germicidal properties; however it is almost entirely filtered out by the Earth’s atmosphere. Therefore, to utilize the germicidal properties of UVC light, it must be artificially generated using manufactured light sources.

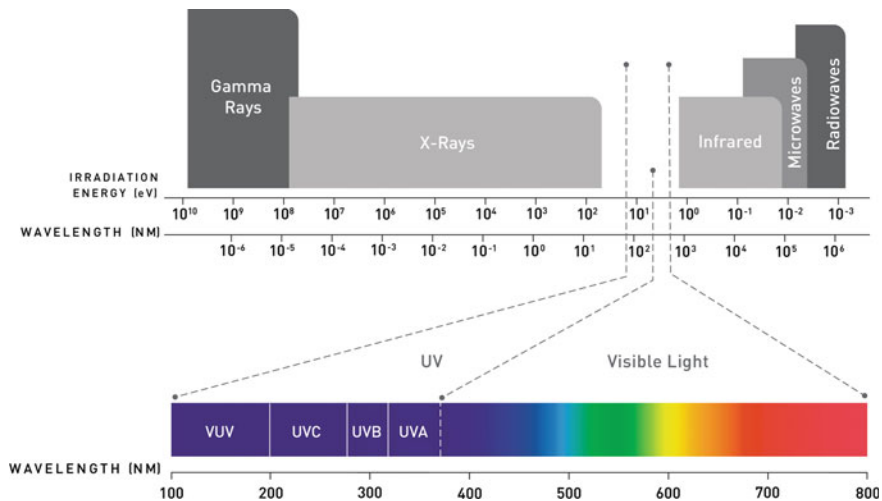


Fig. 7.1 Electromagnetic spectrum

Table 7.1 Comparison of UVC LEDs with other UV technologies

	UVC LED	Deuterium lamp	Xenon flash lamp	Mercury lamp
Spectrum	Single peak	Broad spectrum	Broad spectrum	Broad spectrum
Stability of light output	Excellent	Good	Relatively poor	Relatively poor
Warm up time	Instantaneous	20–30 min	Instantaneous	1–15 min
Forward heat radiation	No	Yes	No	Yes
Overall cost of ownership	Low ^a	High	High	Low
Drive electronics	Simple	Complex	Complex	Complex
Environmentally friendly	Yes	No	No	No
Safety	Low voltage, cold light source with shock resistant construction	Hot bulb surface with high voltage power supply	High voltage supply with ignition and sparking risk	High voltage supply and contains mercury in fragile quartz envelope

^aLowered cost of ownership due to cost savings on power supply and housing

Although UVC LED technology is new, it holds many benefits over the existing UVC technologies (Table 7.1).

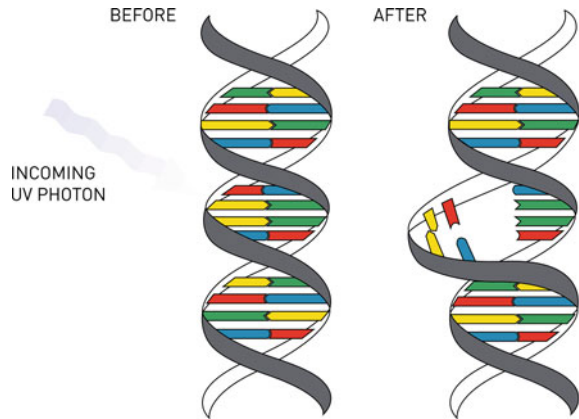
UVC LEDs have many advantages over other technologies that produce UVC light. UVC LEDs come on instantaneously and are well suited for situations where the radiation can advantageously be switched on and off quickly. Also, the lifetime of the LEDs are not degraded by multiple on and off cycles, unlike mercury lamps where the lifetimes decrease with frequent on/off cycles. Another significant benefit for using LEDs is the simplified drive electronics needed to operate them compared to other UVC sources.

Some applications, such as analysis of heat-sensitive samples, also benefit from the lack of forward heat radiation from LEDs. Backside waste heat from LEDs is removed by thermal conduction, typically from the backside, unlike other UVC light sources where it is radiated forward with the UVC light.

7.1.3 How Does Germicidal UV Work

The UVC wavelength range deactivates bacteria, viruses, and other pathogens by attacking their DNA. UVC light is able to penetrate the cells of microorganisms and disrupt the structure of their DNA molecules (Fig. 7.2) [7]. In doing so, the microorganism is prohibited from surviving and/or reproducing, thereby, rendering it inactive and no longer pathogenic.

Fig. 7.2 UVC Radiation disrupts DNA (from [7] by David Herring, NASA, open source)



Mercury lamps, both low pressure and medium pressure, are currently widely used for disinfection. However, in point-of-use (POU) water disinfection, UVC LED technology has become more interesting as output powers and wall plug efficiencies have improved over the last few years. Also, UVC LEDs can be tuned to a desired wavelength, allowing them to provide maximum power at 265 nm—the ideal wavelength for disinfection of most pathogens.

Given the potential advantages of UVC LEDs, it is not surprising that there is an international development effort based on the AlN/GaN compound semiconductor system, more commonly referred to as the III-nitride semiconductors. The majority of this work has involved heteroepitaxial growth of alloys of these semiconductors grown on sapphire substrates by either organometallic vapor phase epitaxy (OMVPE) or molecular beam epitaxy (MBE). While sapphire substrates are capable of meeting the temperature and chemical compatibility requirements for heteroepitaxial growth of the III-nitride semiconductors (and is described elsewhere in this book), the large lattice and thermal expansion mismatch results in a high defect density, which lowers the performance of the resulting UVC LEDs. The number of defects in the heteroepitaxial layers can be dramatically reduced through special epitaxial growth techniques (also described elsewhere in this book). However, higher quality layers of high aluminum content III-nitride semiconductors can be grown pseudomorphically on AlN substrates.

7.2 Fabrication of UVC LEDs on AlN Substrates

Pseudomorphic growth of AlGaN structures on AlN substrates has produced LEDs with dislocation densities much lower than achievable with conventional heteroepitaxy on sapphire or SiC [8]. In order to define a pseudomorphic limit, various growths were carried out with different compositions and thicknesses [9]. This included n-type $\text{Al}_x\text{Ga}_{1-x}\text{N}$ with x from 0.45 up to 0.75 and thickness values

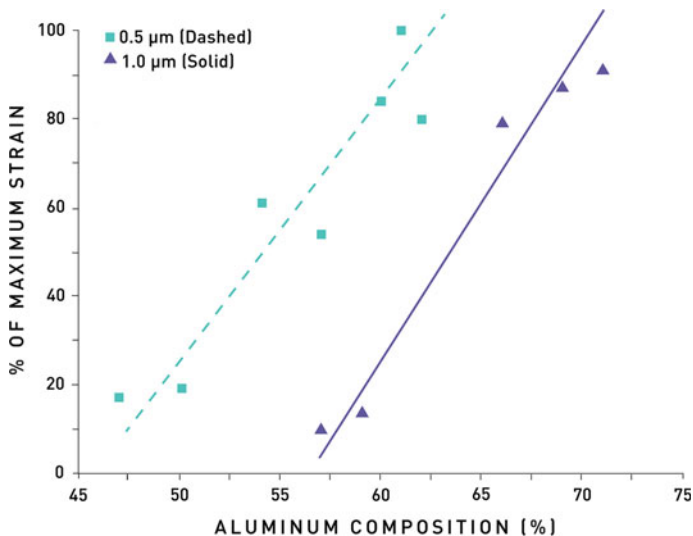


Fig. 7.3 Percent of maximum (pseudomorphic) strain versus Al composition for different thickness layers. The lines are guides to the eye for each thickness (*dashed line* is 0.5 μm and *solid line* is 1.0 μm) [8]

from 0.5 to 1.3 μm thick. In this range, layers found were nearly completely relaxed to completely strained. A plot of the data is shown in Fig. 7.3. As it can be seen, layers of $\sim 60\%$ Al can be grown fully pseudomorphic up to a thickness of 0.5 μm while layers of $\sim 70\%$ Al can be grown nearly pseudomorphic up to a thickness of 1 μm . There is a considerable spread in the data, which could be due to the properties of the AlN substrates, such as surface miscut.

The main advantage to the pseudomorphic growth is that, since no misfit dislocations are generated, no new threading dislocations will need to be generated. Additionally, it is possible to grow thick layers with a threading dislocation density (TDD) comparable to the starting substrate. X-ray rocking curves are shown in Fig. 7.4a for a pseudomorphic layer and in Fig. 7.4b for a relaxed layer. These rocking curves are normalized and plotted with the omega axis shifted to allow for overlaying the $\text{Al}_x\text{Ga}_{1-x}\text{N}$ peak over the AlN peak. For the pseudomorphic sample, the (0 0 0 2) rocking curve width increases from 64 s for the AlN to 81 s for the $\text{Al}_x\text{Ga}_{1-x}\text{N}$ layer while the (10 $\bar{1}$ 2) rocking curve width increases from 89 to 104 s.

This is in sharp contrast to the relaxed sample in which the (0 0 0 2) rocking curve width increases from 49 s for the AlN to 239 s for the $\text{Al}_x\text{Ga}_{1-x}\text{N}$ layer while for the (10 $\bar{1}$ 2) rocking curve width increases from 30 to 302 s. From these scans, it can be seen that by appropriately controlling the Al composition and thickness, very few dislocations are generated during the heteroepitaxy. By keeping the Al composition fixed at 70% and between 0.5 and 1.0 μm thick, layers can routinely be grown with both symmetric and asymmetric rocking curves less than 100 arc sec. In addition to the narrow rocking curves, it is also important for the n-type $\text{Al}_x\text{Ga}_{1-x}\text{N}$

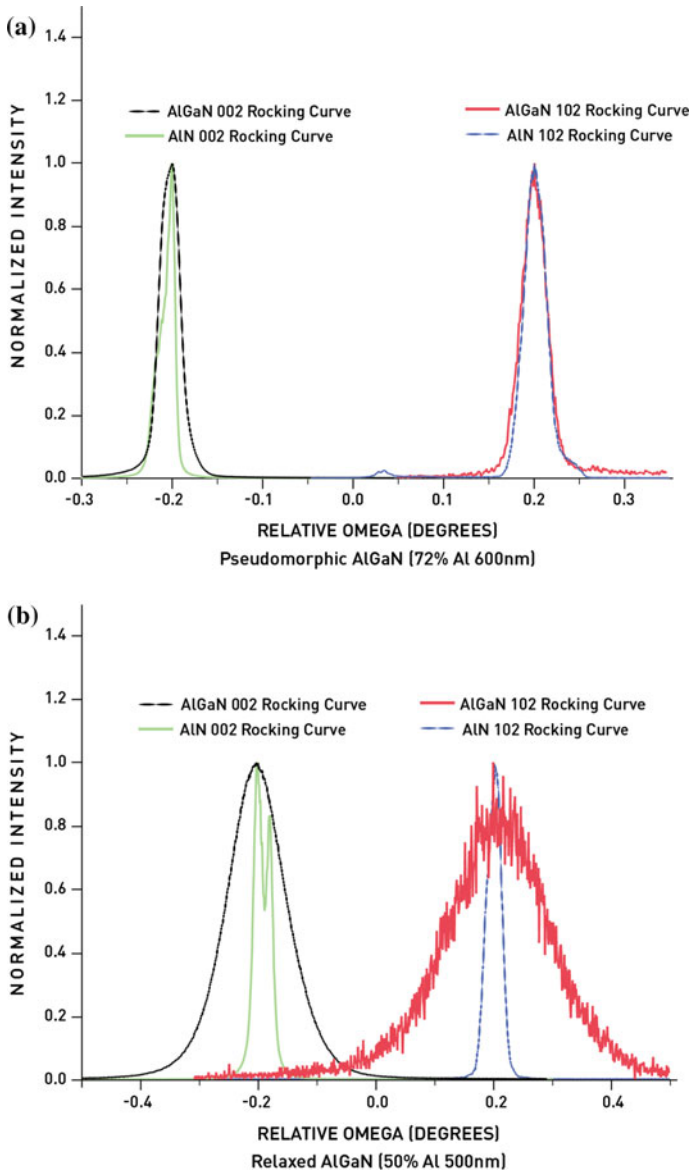
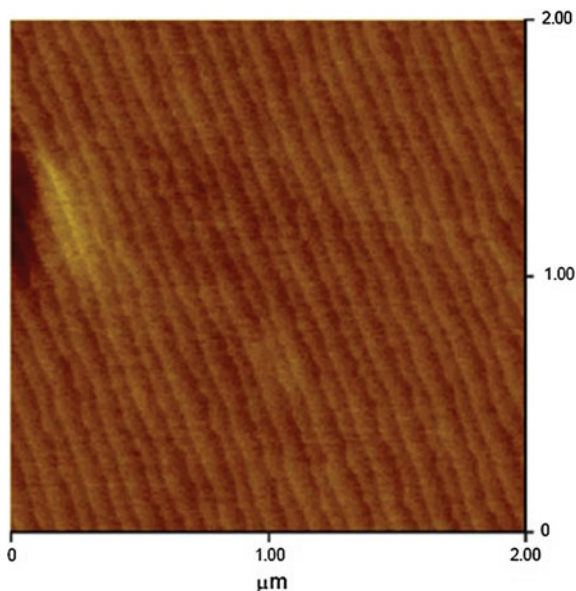


Fig. 7.4 X-ray rocking curves of the AlN substrates and $\text{Al}_x\text{Ga}_{1-x}\text{N}$ epitaxial layers for **a** pseudomorphic layer and **b** relaxed layer. The data is normalized and the X-axis is plotted in relative degrees to allow for the overlaying of the symmetric and asymmetric peaks for AlN and $\text{Al}_x\text{Ga}_{1-x}\text{N}$ [8]

Fig. 7.5 A $2 \times 2 \mu\text{m}^2$ AFM scan showing the step flow growth of the pseudomorphic n-type $\text{Al}_x\text{Ga}_{1-x}\text{N}$ layer with a composition of 70 % Al. The RMS roughness is 0.1 nm and the Z-range is 1.7 nm (for a $20 \times 20 \mu\text{m}^2$ scan the RMS roughness is 0.4 nm and the Z-range is 2.1 nm) [8]



to have smooth surfaces in order to provide sharp interfaces in the p–n junction and thin active region. It was found that layers begin relaxing by a surface roughening mechanism. Initially, the surface appears to buckle to reduce the compressive strain in the layers. Upon continued growth, very rough surfaces were obtained for the $\text{Al}_x\text{Ga}_{1-x}\text{N}$ layers with 60 % Al at $0.5 \mu\text{m}$ thick. This is similar to what was seen previously in the growth of lower composition $\text{Al}_x\text{Ga}_{1-x}\text{N}$ on low dislocation density bulk AlN substrates in which plateaus develop on the surface [10]. However, the $\text{Al}_x\text{Ga}_{1-x}\text{N}$ layers with 70 % Al can be grown with very smooth surfaces as seen in Fig. 7.5.

This step flow growth pattern with atomically smooth surfaces is typical over large areas with $20 \times 20 \mu\text{m}^2$ scans showing similar Z-range and RMS values (not shown). One challenge of incorporating this 70 % Al $\text{Al}_x\text{Ga}_{1-x}\text{N}$ layer into an LED structure is the conductivity. As the Al concentration is increased, the conductivity is typically decreased, due mainly to the reduced mobilities [11] and deeper level of the donor in the conduction band [12]. Hall measurements were performed in the Van der Pauw geometry and gave conductivity values suitable for an LED structure, a resistivity of $0.0437 \Omega \text{ cm}$ with a mobility of $62 \text{ cm}^2/\text{V s}$ at a carrier concentration of $2.4\text{E}18 \text{ cm}^{-3}$. These values were obtained without any optimization of the doping levels or growth conditions and it is expected that improved conductivity can be obtained.

The next step in obtaining a full LED structure is the growth of the Multiple Quantum Wells (MQW) [13]. This was carried out on the smooth 70 % Al $\text{Al}_x\text{Ga}_{1-x}\text{N}$ layer. The step flow growth mode and atomically smooth surfaces continued during growth of the MQW and the surface roughness was similar to that of the 70 % Al

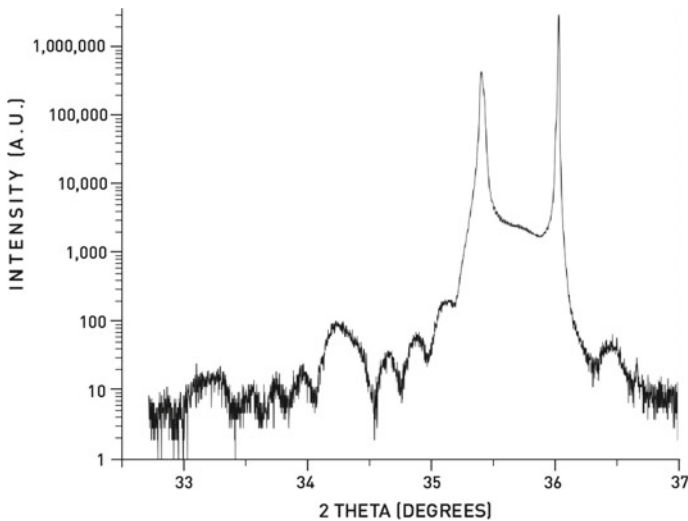
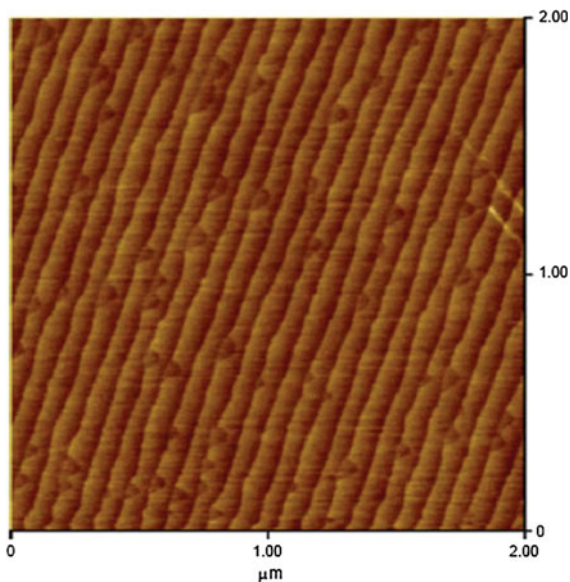


Fig. 7.6 Omega-2 theta scan of the MQW structure showing the sharp AlN and 70 % Al_xGa_{1-x}N layer as well as the interference fringes from the MQW [8]

Al_xGa_{1-x}N layer. XRD was carried out on this structure and is shown in Fig. 7.6. In addition to the sharp peaks coming from the AlN substrate and the 70 % Al Al_xGa_{1-x}N layer, interference fringes are observed from the MQW allowing measurement of the compositions and thickness of the well and barrier layers which matched very well to the desired structure. Finally, a full LED structure was grown consisting of a high Al-content electron blocking layer, a p-type Al_xGa_{1-x}N hole injection layer and a p-type GaN contact layer. The device structure was grown on c-plane AlN substrates using conventional metal organic chemical vapor deposition. It consists of an Al_{0.7}Ga_{0.3}N:Si layer, a five period multiple quantum well (MQW) layer consisting of n-Al_{0.7}Ga_{0.3}N barriers and Al_{0.55}Ga_{0.45}N wells, an Al_{0.8}Ga_{0.2}N electron blocking layer (EBL), and a p-GaN contact layer [14]. Again, step flow growth continued as can be seen in Fig. 7.7. XRD (not shown) also showed narrow GaN peaks indicating that the low defect density is carried throughout the entire structure. This improvement in both defect density and surface roughness is expected to lead to dramatic improvements in device structures fabricated into UVC LEDs.

While the epitaxial material quality is improved due to the low dislocation density, one issue with the use of AlN substrates prepared from bulk crystals is absorption of the UV light generated even though the crystal quality is very high. While intrinsically transparent at these wavelengths, point defects in the bulk substrates can result in absorption, many times resulting in opaque substrates. One technique that has been used to achieve substrates with high transparency is HVPE AlN growth on PVT grown AlN substrates. HVPE growth can achieve low impurity incorporation and is able to closely replicate the underlying high quality substrate with low dislocation density. This technique was demonstrated successfully with a

Fig. 7.7 A $2 \times 2 \mu\text{m}^2$ AFM scan showing the step flow growth of the full LED structure (p-type GaN contact layer). The RMS roughness is 0.2 nm and the Z-range is 1.6 nm (for a $20 \times 20 \mu\text{m}^2$ scan the RMS roughness is 0.2 nm and the Z-range is 2.0 nm) [8]



28 mW measurement from a 268 nm LED [15] after removing the PVT substrate with an applied current of 300 mA.

Recently, it has been demonstrated that pseudomorphic growth of UVC LEDs gives improved reliability. The LED structures were grown by metal organic chemical-vapor deposition (MOCVD) on free standing AlN substrates as described above [16]. Devices were fabricated via standard lateral LED processing, with a final die size of $820 \mu\text{m}$ by $820 \mu\text{m}$. Interdigitated mesas were used to improve current spreading, and the emitting area was approximately $0.37 \mu\text{m}^2$. Following contact metallization, but prior to singulation, the substrate was thinned to $200 \mu\text{m}$. After flip-chip bonding, some LEDs were further thinned to approximately $20 \mu\text{m}$. One of two packaging options was used depending on the LEDs eventual use, either a lead frame package for high-power measurements or a hermetically sealed TO-39 package with a ball lens to provide a nearly collimated beam for instrumentation applications. Lead frame devices were encapsulated to improve extraction efficiency [17]. All devices were mounted to heat sinks for optimal thermal dissipation.

Figure 7.8 shows recent L-I results for two LEDs with peak wavelengths of 266 and 278 nm, as independently measured by the US Army Research Laboratory (ARL) [18]. The LEDs were driven in both continuous wave and pulsed modes. The two current input methods diverge only slightly beginning above 150 mA as device self-heating begins to limit the output power of the continuously driven LED. In pulsed operation, there is a minimal drop in external quantum efficiency up to current densities of 120 A/cm^2 .

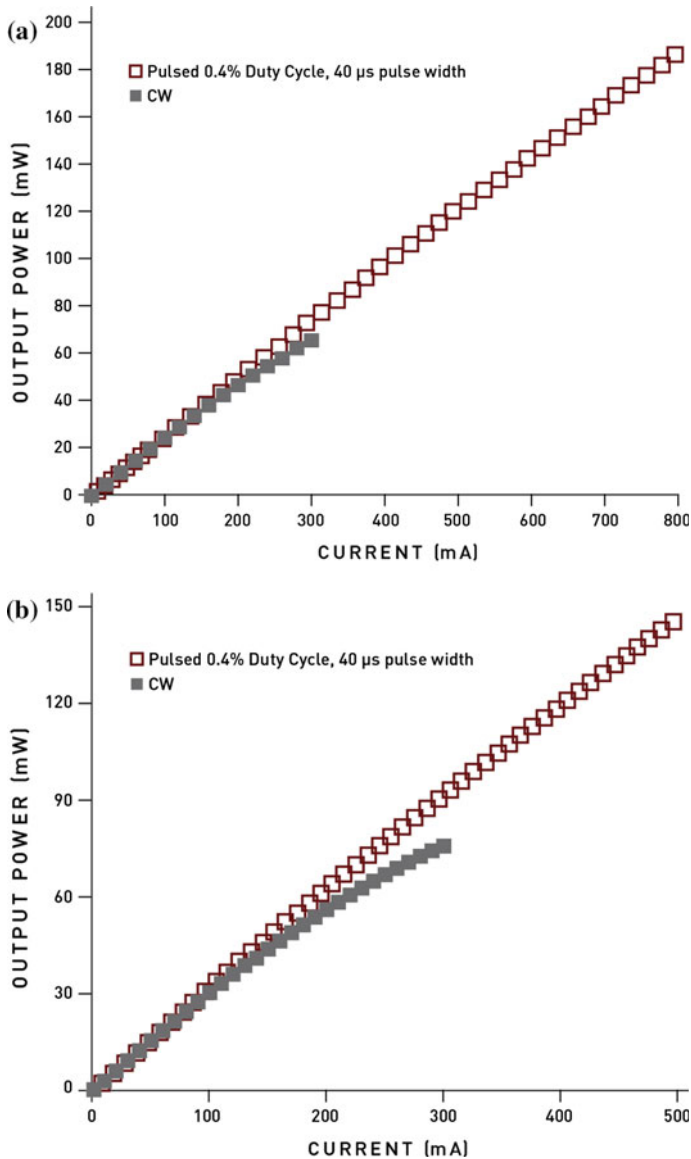


Fig. 7.8 L-I curves for 266 **a** and 278 nm; **b** LEDs under CW and pulsed conditions as measured by the U.S. Army Research Laboratory [18]

Absorption of ultraviolet light in the substrate remains a source of concern. Though the larger band gap of AlN should allow for transmission of UV down to 205 nm, defects and impurities introduced in the bulk crystal growth process can produce significant substrate absorption. We observe an absorption peak centered around 265 nm, with a peak value ranging from 20 to 85 cm^{-1} for the substrates

used in this work. Thinning of the substrate to 200 μm increases the measured output power by roughly 2 \times , while further thinning to 20 μm increases light extraction by another 2 \times .

In spectroscopic applications, the ratio of peak wavelength emission to light at longer wavelengths impacts measurement quality. Many biological compounds measured in these applications are excited by UVC wavelengths and produce light in the longer wavelengths. Autofluorescence describes the phenomena of light absorption and reemission by the LED substrate. Stray peaks emitted by the LED at these longer wavelengths can diminish accuracy in absorption and fluorescence spectroscopy. High quality UVC LEDs with a lower absorbing substrate will reduce the magnitude of this auto fluorescence.

The autofluorescence ratio was measured on a sample of UVC LEDs where the substrate had been thinned to 20 μm . For the devices displayed in Fig. 7.8 measured at ARL, the peak-to-325 nm emission ratio was 1,000, and the peak-to-400 nm emission was 2,000 at 10 mA drive current. When measured at Crystal IS, the same devices showed ratios of 3,000 at 100 mA (a difference seen due to signal-to-noise ratios). A sample of 721 diodes with thicker substrates, where the chance of re-emission is increased, showed peak-to-visible emission ratios greater than 100.

Pseudomorphic growth results in improvements to reliability. Figure 7.9 shows a histogram of the relative output power of 170 lead frame packaged LEDs after 1,000 h of CW operation at 100 mA. The median LED emits 97.2 % of its initial output power. Twenty-one devices (12.4 %) emit less than 40 % of their initial output power. The latter devices are primarily clustered around 0, indicating catastrophic failures due to a malfunction of the contact metallization or packaging. Analysis of the failed devices showed corrosion and metal migration, often exacerbated by environmental conditions. A sample of 40 devices in a hermetically sealed TO-39 package showed no failures of this nature.

In conclusion, improvements in device design have produced UVC diodes with more consistent emitting wavelength, reliability, and emission peak fidelity without sacrificing efficiency gains. AlN substrate absorption has a significant effect on

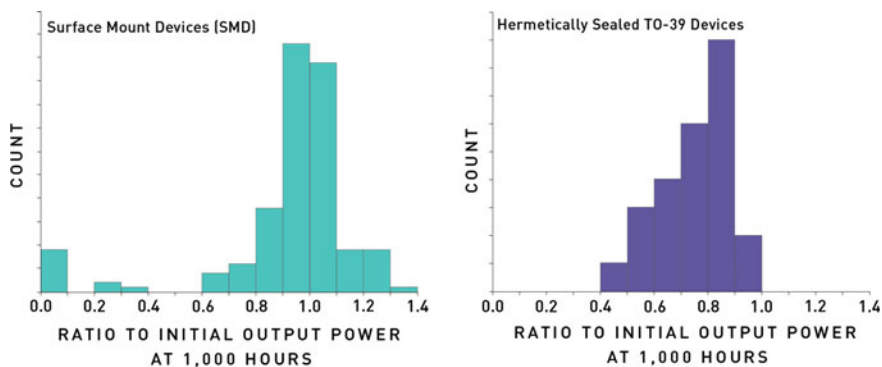


Fig. 7.9 Histogram of relative output power after 1,000 h operation at 100 mA for LEDs in an SMD (*left*) and hermetically sealed TO-39 package (*right*)

on-wafer results, but can be mitigated in the final device with advanced manufacturing techniques. Packaging improvements can also eliminate catastrophic failures in devices and allow for consistent device lifetimes with L_{50} values in excess of 1,000 h.

7.3 Leveraging Performance Gains in UVC LEDs for POU Water Disinfection

The performance gains in recent UVC LEDs have increased the interest in using these light sources for point-of-use (POU) water disinfection systems. In designing these systems, consider the following factors:

- (a) Water Quality
- (b) Flow cell dimension
- (c) Dosage
- (d) Material of construction
- (e) Pathogen(s) to be inactivated
- (f) Thermal management

What follows is a discussion on guiding principles for each of these factors.

(a) *Water Quality*

Water quality is critical in determining the amount of UVC light needed for disinfection. Of all water quality parameters, ultraviolet transmissivity (UVT) is the most important. The UVT of the water determines how well the UVC light will penetrate into the water, ensuring pathogens in the water are exposed to sufficient UVC light to be inactivated. Particles can reduce UVC disinfection capability by shielding microbes and absorbing UVC light. The use of filters will remove these suspended particles prior to UVC treatment.

As a general rule, a UVC unit would be installed in series following a filtration unit. If the reverse were implemented—that is, UVC unit then filter—higher UVC doses would be required to achieve the same level of inactivation, due to higher levels of Natural Organic Matter (NOM) turbidity and particulate matter.

7.3.1 *Effect of UVT*

UVT describes the amount of UV light passing through water according to the following:

$$\%UVT = 100 \times 10^{(-A_{254} * d)}$$

where:

- UVT UV transmittance at a 254 nm and a 1 cm path length
 A₂₅₄ UV absorbance at 254 nm based on a 1 cm path length
d distance from UV lamp (cm)

Turbidity, particulate matters, and organic matter in the water affect the UVT. As the turbidity increases, UVT decreases and as UVT decreases, UV intensity delivered to the microorganism decreases [19].

(b) *Flow Cell Dimension*

The efficiency of a UVC disinfection system depends on the size of the flow cell. The size is often dictated by the space available in a particular design and the amount of water requiring disinfection. These dimensions determine the amount of optical power required for disinfection.

The tube dimension and flow rate are used to calculate the residence time of the microbe(s) in the flow cell. Typical flow rates for point-of-use application are about 1 gallon per minute and point-of-entry systems can have flow rates between 1 and 8 gallons per minute.

(c) *Dosage*

A key factor in determining how effective UVC light will be in deactivating a given pathogen is the dosage that the pathogen in the water receives. The dosage is defined as the intensity of the UV light times the residence time:

$$\text{UV Dose} = \text{Intensity } (I) \times \text{Residence time } (t)$$

where Intensity (*I*) is measured in milliwatts per cm² (mW/cm²) and Exposure time (*t*) is measured in seconds (s).

The longer the residence or exposure time, the more UVC radiation will penetrate the pathogen's cells, and therefore, the more effective the inactivation process will be. The slower the flow rate of the water through the UVC system, the longer the UVC exposure time, and vice versa. Therefore, considering the maximum necessary and minimum allowable flow rate of the water in a particular system is a determining factor for setting the power requirement for the application.

(d) *Material of Construction*

The material used for the flow cell will impact the system efficacy. For example, materials with highly reflective properties for the UVC light will enhance its effectiveness. A list of materials with varying reflectance of UVC light, specifically around 250 nm, is available from the International Ultraviolet Association (IUVA) [20].

The most common material currently used in mercury lamp-based systems is stainless steel, although it only has 28–33 % reflectance [20]. Considering materials containing e-Polytetrafluoroethylene [20], which has over 90 % reflectance in the

UVC range, may create a much more effective system. Polished aluminum also has high UVC reflectance. It is, however, sometimes unacceptable for reactor designs due to leaching of Al ions.

(e) *Pathogen(s) to be inactivated*

Another factor to consider is the type of microorganism that needs to be inactivated. Different pathogens have differing resistance to UV; some are more susceptible than others and so require different amounts of exposure to inactivate them. In order to correctly size and select a UV system, it is generally recommended to establish which pathogen(s) are to be targeted.

It is common for microbe inactivation to be measure on a logarithmic scale. Thus, a “one log,” or 1 log, reduction describes pathogen reduction of 90 % from the influent level. A 2 log reduction describes a 99 % reduction, 3 log by 99.9 %, and so on. The dosage required for the inactivation has historically been measured only for low or medium pressure mercury lamps. Achieving the same log reduction using UVC LEDs requires proper testing.

Scientists have calculated the amount of UV exposure required to inactivate a whole range of different pathogens by various log reductions. NSF 55 standard describes requirements for meeting point-of-use and/or point-of-entry water disinfection specifications [21]. Class A requirements, which corresponds to 6 log reduction of bacteria, 4 log for virus and 3 log for *Giardia*, specifies a dosage of 40 mJ/cm² based on the spectrum of the standard mercury lamp. Class B, which corresponds to reduction of most all nuisance microbes, specifies a 16 mJ/cm².

(f) *Thermal Management*

When voltage or current is applied across the junction of an LED, the input electrical energy is converted into light and the rest into heat. The cooler the LED is kept, the better the performance—as seen in Fig. 7.10 for light output versus temperature. Managing the heat conduction path from the backside of an LED will promote optimal performance in LED-based applications.

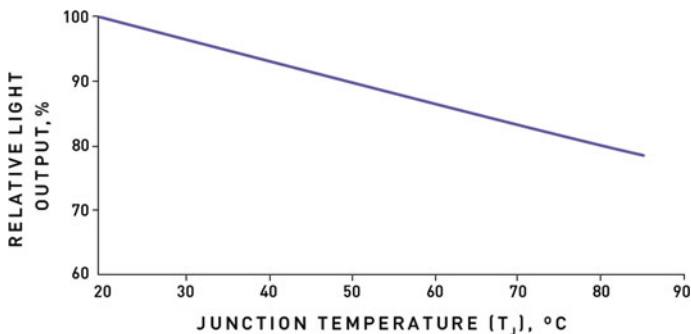


Fig. 7.10 Effect of light output as a function of junction temperature

The amount of electrical energy that is converted to heat (P_D) can be estimated by using the parameters, forward voltage (V_f), applied current (I_f), and the LED wall plug efficiency (WPE), and it is represented in the equation below.

$$P_D = V_f * I_f * (1 - \text{WPE})$$

This means that if the Wall Plug Efficiency is 1 % for UVC LEDs, then 99 % of the input electrical power needs to be removed as heat.

Figure 7.10 shows the impact on optical power output if the junction temperature of the LED is allowed to increase due to heat that is generated from the operation of the LED. The junction temperature can be maintained by having an appropriate heat sink. If operating conditions call for further improvement of the thermal transfer beyond this simple passive heat sink-to-air interface, then fans may be added to the system to force convection and move cooler air between the fins. Other such active cooling techniques include the treated water from the flow cell and heat pipes to enhance thermal transfer [22].

7.3.2 *Design Flexibility*

Once the key application requirements are known, a system can be considered to achieve a targeted level of UVC disinfection. As extremely compact light sources, a major advantage of LEDs is that they can be incorporated into almost any design, theme, or object. Unlike traditional UVC sources, such as mercury lamps that only offer a single tube format, LEDs are a point source and can be used in applications in a variety of ways. The small size, scalability of arrays, and directional light emission of LEDs can be easily and ideally suited for use in linear, flat, or round area applications. For example, a traditional flow cell system for water disinfection places a mercury lamp in the center of a stainless steel tube with a quartz tube around the bulb as shown in the Fig. 7.11a. In the case of LEDs, there are number of different possibilities for mounting depending on the flow rate. Figure 7.11b–d illustrates varied placements for LEDs in end caps of the tube, on the outside of the flow cell, or as vertical arrays on the inside of the tube.

7.3.3 *Modeling Flow Cells*

It is generally desirable to maximize the water residence time in a flow cell. Computational fluid dynamics (CFD) is a useful tool to understand the flow constraints of a particular design. Optical modeling may also be used to examine various arrangement and location possibilities for LEDs in a given system. An optical model can be a guide for proper arrangement of diodes to have the flow cell

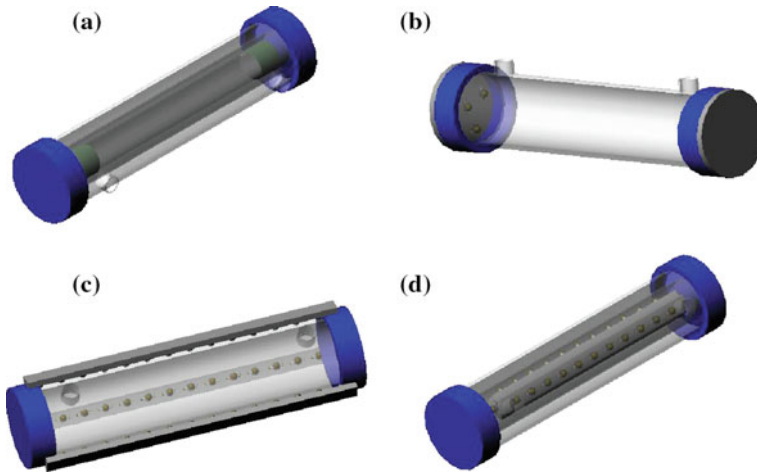


Fig. 7.11 a Flow Cell with center-mounted mercury lamp; b flow cell with LEDs mounted in end caps; c flow cell with LEDs positioned outside UV transparent tube; d flow cell with LEDs array mounted inside

completely illuminated with maximum uniformity and determine the minimum and maximum irradiance values experienced.

7.3.4 Example Flow Analysis

The following example outlines a process for developing a flow cell for UVC disinfection using UVC LEDs. The process starts with a flow analysis for the given application.

The calculations for the flow pattern were carried out using open CFD software called OpenFOAM [23]. The flow pattern will help determine the shortest and the mean time it takes for a microbe to pass through the flow cell. This provides the amount of irradiance needed to meet the NSF 55 requirement of 6 log reduction for bacteria, 4 log for Virus, and 3 log for protozoa.

This example evaluates three different flow cells (Fig. 7.12) with the same dimensions, but different internal designs to increase the residence time of the microbe in the flow cell.

These flow cell designs were modeled to determine the shortest and mean flow once the water entered into flow cell to its exit point. This provides the time the typical microbe stays in the flow cell and determines the appropriate amount of UVC light required to inactivate the microbe. The streamlines for possible flow paths can be modeled for each flow cell. The total residence time is calculated based on these streamlines. Figure 7.13a-1, b-1, c-1 show the streamlines for of the three different flow cells from Fig. 7.12. The single streamline shown in Fig. 7.13a-2, b-2, c-2 illustrate the direct path for water to flow from inlet to outlet.

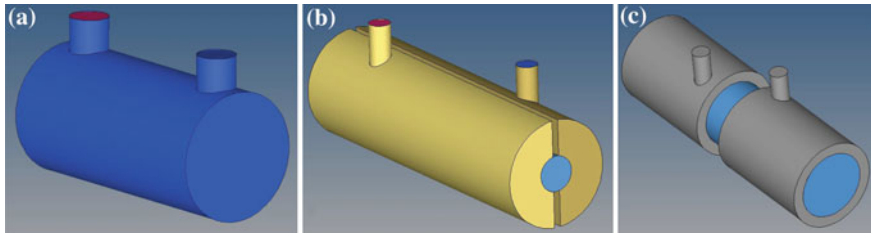


Fig. 7.12 Different flow cell conceptual designs with same volume

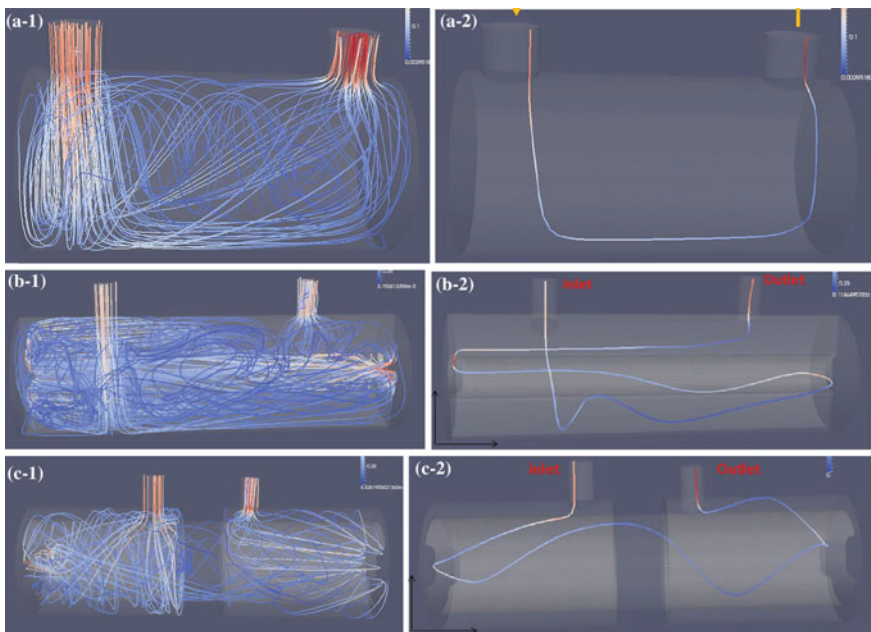


Fig. 7.13 The models show the streamline for water flow using OpenFOAM software for the three different flow cells

The modeling suggests a mean path of a target microbe in different flow cell designs. The table below shows calculations for the minimum and mean hold up times compared to the ideal flow time for the three concepts (Table 7.2).

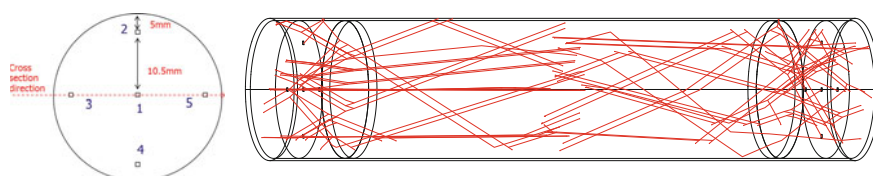
The minimum hold up time is similar across all three flow cell concept designs. However there is variation in the mean hold up time. In this example, concepts B and C appear more desirable as they maximize the residence time of water in the flow cell.

Further analysis through Zemax[®] optical modeling helps to predict the pattern of light emission in the flow cell. Figure 7.14 shows the optical model for Fig. 7.11b with the lowest mean holdup time. Using the arrangement of LEDs placed in end caps on the flow cell, the model was used to predict the irradiation pattern on the

Table 7.2 Calculations for the minimum and mean hold up times compared to the ideal flow time for the three flow cell concepts

Model	Minimum holdup (s)	Ratio (to ideal ^a flow)	Mean holdup (s)	Ratio (to ideal ^a flow)
Concept A	1.16	0.39	3.09	1.03
Concept B	1.19	0.40	3.84	1.27
Concept C	1.12	0.37	3.76	1.25

^aWater flow time in flow cell based on theoretical calculations of 3 s

**Fig. 7.14** Location of diodes mounted in the end cap and the optical model for light in the flow cell with the lowest mean hold up time

flow cell. Figure 7.15a, b shows the slice view of the optical model—both near the end cap and in the center of the flow cell.

Once the optical modeling was complete, the flow cell and circuitry was manufactured. The circuit boards were mounted to the proper heat sink to maintain the thermal management of the system. Once completely assembled, biological testing was performed based on EPA (Environmental Protection Agency) protocol [24].

Based on the CFD modeling for the water flow pattern and the optical modeling it was decided to manufacture two flow cells, the best case and worst case—Concept A and Concept C. Comparing these extremes shows the importance of residence time. Tests were performed at three flow rates with a UVT of 90 % and a single power input (100 %). Each test used samples taken of the influent and effluent. The influent was seeded with T1 and MS2 coliphage, and the bench test influent and effluent samples were analyzed for each phage surrogate.

The resulting data is represented in Fig. 7.16 for MS2 and T1 bacteriophage.

The data shows that Concept C has higher log reduction for both MS2 and T1. Based on the CFD modeling, it was predicted that Concept C would have a higher mean hold up time compared to Concept A. The optical model showed the amount of light in the flow cell and the optical power was consistent for both flow cells. Thus, the data reveals that the main parameter for increased log reduction was the holdup time—or rather the residence time. If the flow cell with a longer residence time is designed, the disinfection of the water is maximized.

7.3.5 Working with UVC Light

This chapter has discussed some of the design principles to take into account while designing a flow cell for POU water disinfection using LEDs, as well as illustrating

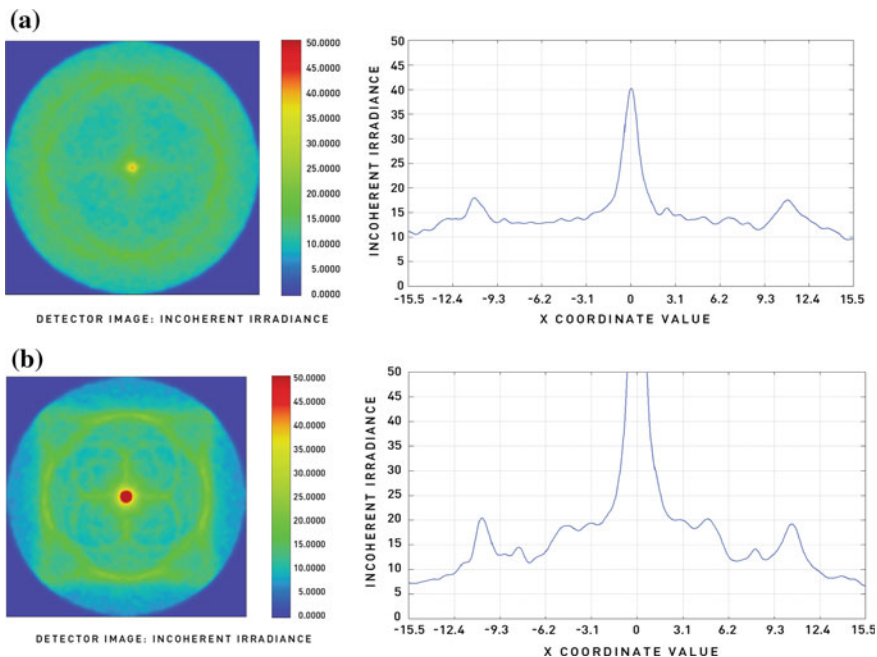


Fig. 7.15 Shows the slice view of the optical model. **a** Near the end cap and **b** in center of the flow cell

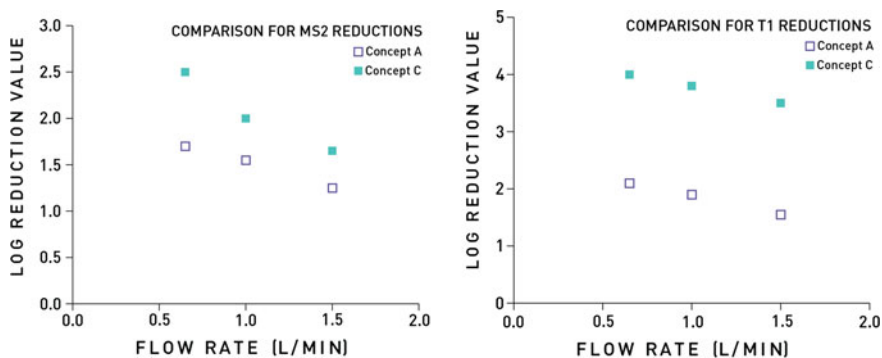


Fig. 7.16 Comparison for concept A and concept C for flow cell for MS2 and T1 reductions

how modeling and testing can be performed to validate these principles. Additionally, there are precautions that need to be taken with an operational unit.

(a) *Fouling of quartz window in front of UVC source*

A quartz window allows the UVC light to reach the water while protecting the LEDs and circuitry from water damage. Fouling of this quartz window, also known

as lamp jacket fouling, could occur due to the hardness of the water and/or presence of iron in the water. If this occurs, the amount of UVC light getting into the system is reduced and would potentially reduce disinfection.

Surface fouling is problematic because it absorbs UVC irradiation, reducing the dose applied to the water treated, and is most significant in waters with high concentrations of dissolved metals. One suspected precursor to lamp jacket fouling is aqueous phosphate [25]. Phosphates are often added to drinking water to aid in sequestering dissolved metals and prevent distribution network corrosion. However, orthophosphate and condensed phosphates have the potential to speed lamp jacket fouling by combining with dissolved metals and precipitating onto lamp jacket surfaces.

(b) *Monitoring UVC light output*

Monitoring UV light ensures that the right dosage for meeting desired disinfection requirements is occurring. A UVC monitor will detect the levels of light output in the system and let the end user know the unit is operating efficiently. The design can incorporate some existing optometer that measures in the UVC range, or create an additional circuit using a silicon-based pin diode.

(c) *Safety*

Depending on the length of exposure, UVC light can have adverse effects on human skin and eyes. UVC light exposure can be easily prevented during development, testing, and operation if proper precautions are put in place. The American Conference of Governmental Industrial Hygienist (ACGIH) [26] provides guidelines on use of proper PPE and permissible limits for exposure for individuals.

Including safety design controls for the equipment in-use is almost always a key aspect of design. Likewise, performing routine maintenance of the equipment and providing the proper training when working with UVC light is advisable.

References

1. http://whqlibdoc.who.int/publications/2008/9789241596435_eng.pdf
2. W. Heering, UV Sources-basics, properties and applications. *IUVA News* **6**(4) (2004)
3. M.A. Wurtele, T. Kolbe, M. Lipsz, A. Kulberg, M. Weyers, M. Kneissl, M. Jekel, Application of GaN-based ultraviolet-C light emitting diodes UV LEDs for water disinfection. *Water Res.* **45**:1481–1489 (2011)
4. J.R. Grandusky, J. Chen, S.R. Gibb, M.C. Mendrick, C.G. Moe, L. Rodak, G.A. Garrett, M. Wraback, L.J. Schowalter, *Appl. Exp. Lett.* **6** (2013)
5. R. Schaefer, M. Grapperhaus, I. Schaefer, K. Linden, Pulsed UV lamp performance and comparison with UV mercury lamps. *J. Environ. Eng. Sci.* **6**, 303–310 (2007)
6. B.L. Diffey, Sources and measurement of ultraviolet radiation. *Methods* **28**, 4–13 (2002)
7. http://www.nasa.gov/topics/solarsystem/features/uv-exposure_prt.htm
8. J.R. Grandusky, J.A. Smart, M.C. Mendrick, L.J. Schowalter, K.X. Chen, E.F. Schubert, Pseudomorphic growth of thick n-type $\text{Al}_x\text{Ga}_{1-x}\text{N}$ layers on low-defect-density bulk AlN substrates for UV LED applications. *J. Cryst. Growth* **311**, 2864 (2009)

9. J.Z. Ren, Q. Sun, S.Y. Kwon, J. Han, K. Davitt, Y.K. Song, A.V. Nurmikko, H.-K. Cho, W. Liu, J.A. Smart, L.J. Schowalter, *Appl. Phys. Lett.* 91, 051116 (2007)
10. A.A. Allerman, M.H. Crawford, A.J. Fischer, K.H.A. Bogart, S.R. Lee, D.M. Follstaedt, P. P. Provencio, D.D. Koleske, *J. Cryst. Growth* 272, 227 (2004)
11. J.T. Xu, C. Thomidis, I. Friel, T.D. Moustakas, *Phys. Status Solidi (c)* 2, 2220 (2005)
12. F. Mehnke, T. Wernicke, H. Pingel, C. Kuhn, V. Kueller, A. Knauer, M. Lapeyrade, M. Weyers, M. Kneissl, Highly conductive n-AlxGa1-xN layers with aluminum mole fractions above 80 %. *Appl. Phys. Lett.* 1103 212109 (2013)
13. J.R. Grandusky, S.R. Gibb, M.C. Mendrick, C.G. Moe, M. Wraback, L.J. Schowalter, Properties of mid-Ultraviolet light emitting diodes fabricated from pseudomorphic layer on bulk aluminum nitride substrates. *Appl. Phys. Exp.* 3, 072103 (2010)
14. T. Kinoshita, K. Hironaka, T. Obata, T. Nagashima, R. Dalmau, R. Schlessler, B. Moody, J. Xie, S. Inoue, Y. Kumagai, A. Koukitu, Z. Sitar, Deep-ultraviolet light-emitting diodes fabricated on AlN substrates prepared by hydride vapor phase epitaxy. *Appl. Phys. Exp.* 5, 122101 (2012)
15. J.R. Grandusky, S.R. Gibb, M.C. Mendrick, C.G. Moe, M. Wraback, L.J. Schowalter, High output power from 260 nm pseudomorphic ultraviolet light emitting diodes with improved thermal performance. *Appl. Phys. Exp.* 4(8), 082101 (2011)
16. J. Chen, J.R. Grandusky, M.C. Mendrick, S.R. Gibb, L.J. Schowalter, Improved photon extraction by substrate thinning and surface roughening in 260 nm pseudomorphic ultraviolet light emitting diodes, in Lester Eastman Conference on High Performance Devices (2012)
17. J.R. Grandusky, J. Chen, S.R. Gibb, M.C. Mendrick, C.G. Moe, L.E. Rodak, G.A. Garrett, M. Wraback, L.J. Schowalter, 270 nm pseudomorphic ultraviolet light-emitting diodes with over 60 mW continuous wave output power. *Appl. Phys. Express* 6(3), 032101 (2013)
18. C.G. Moe, J.R. Grandusky, J. Chen, K. Kitamura, M.C. Mendrick, M. Jamil, M. Toita, S.R. Gibb, L.J. Schowalter, High-power pseudomorphic mid-ultraviolet light-emitting diodes with improved efficiency and lifetime. *SPIE* 89861V (2014)
19. M. Templeton, R.C. Andrews, R. Hofmann, Particle characteristics influencing the UV disinfection of drinking water, in *Water Quality Technology Conference, American Water Works Association* (2004)
20. <http://iuva.org/sites/default/files/IUVAG01A-2005.pdf>, 50 (2005)
21. <https://www.water2drink.com/resource-center/how-it-works-nsf-testing-standards.asp>
22. https://www.cooliance.com/custom_heatpipes.html
23. <https://www.openfoam.com>
24. Ultraviolet disinfection guidance manual for the final long term 2 enhanced surface water treatment rule; office of water (4601), EPA 815-R-06-007, November 2006
25. I.W. Wait, C.T. Johnston, E.R. Blatchley III, *ASCE* 110, 343 (2004)
26. Ultraviolet Radiation, *ACGIH* (2001)